Minireview

Photoacoustic imaging systems based on clinical ultrasound platform

Eun-Yeong Park[1,2], Haeni Lee[3], Seongyi Han[3], Chulhong Kim[1] iD and Jeesu Kim[3,4]

[1]Departments of Electrical Engineering, Convergence IT Engineering, Mechanical Engineering, and Medical Device Innovation Center, Pohang University of Science and Technology, Pohang 37673, Republic of Korea; [2]Department of Radiology, School of Medicine, Stanford University, Stanford, CA 94305, USA; [3]Department of Cogno-Mechatronics Engineering, Pusan National University, Busan 46241, Republic of Korea; [4]Department of Optics and Mechatronics Engineering, Pusan National University, Busan 46241, Republic of Korea
Corresponding authors: Chulhong Kim. Email: chulhong@postech.edu; Jeesu Kim. Email: jeesukim@pusan.ac.kr

Impact Statement

Photoacoustic imaging is a promising biomedical imaging modality that can visualize structural, molecular, and functional information of the internal body in a real-time, radiation-free, and non-invasive manner. Owing to the inherent similarities between the two modalities, most studies on photoacoustic imaging have been conducted by integrating it into existing ultrasound systems. Because ultrasound imaging is commonly used in current clinical practice, bimodal photoacoustic and ultrasound imaging systems are expected to have relatively lower barriers to clinical translation. However, to be approved as a new medical device, its safety and effectiveness must be ensured through rigorous processes. This review will be helpful in developing a clinical photoacoustic system, implementing clinically useful features, and designing and evaluating a variety of medical diagnostic and therapeutic applications.

Abstract

Photoacoustic imaging has drawn a significant amount of attention due to its unique capacity for functional, metabolic, and molecular imaging, which is achieved by the combination of optical excitation and acoustic detection. With both strengths of light and ultrasound, photoacoustic images can provide strong optical contrast at high ultrasound resolution in deep tissue. As photoacoustic imaging can be used to visualize complementary information to ultrasound imaging using the same data acquisition process, several studies have been conducted on combining photoacoustic imaging with existing clinical ultrasound systems. This review highlights our development of a photoacoustic/ultrasound dual-modal imaging system, various features and functionalities implemented for clinical translation, and preclinical/clinical studies performed by using the systems.

Keywords: Photoacoustic imaging, ultrasound imaging, clinical system, clinical applications, biomedical studies, dual-modal imaging

Introduction

Biomedical imaging techniques, such as X-ray computed tomography (CT), magnetic resonance imaging (MRI), positron emission tomography (PET), single-photon emission tomography (SPECT), optical imaging, and ultrasound imaging (USI), have been widely used in preclinical and clinical studies because visualization is one of the most essential methods in investigating the physiological and morphological responses of biological systems.[1] Among the various imaging techniques, photoacoustic imaging (PAI) has gained particular attention because of its unique advantages in visualizing molecular functional information with relatively good resolution in deep tissue.[2] The cost-efficiency, ease of implementation, and non-ionizing radiation also make PAI favorable for clinical use.

The principles of PAI are based on the photoacoustic (PA) effect, which describes the energy transformation of light to acoustic waves.[3] When a short (typically a few nanoseconds) pulsed laser beam illuminates the target tissue, optical chromophores absorb the light energy. The absorbed light energy is converted to heat, which is rapidly dissipated into the surrounding tissue. Through thermoelastic expansion, rapid heat changes cause rapid expansion and shrinkage of molecules, which generate acoustic waves called PA waves. The generated PA waves are detected by conventional ultrasound (US) transducers and then reconstructed as images through digital signal and image processing algorithms.[4–8]

Regarding the principles of PAI, the data acquisition and image reconstruction parts are identical to those used for USI. Therefore, it is common to combine the two modalities
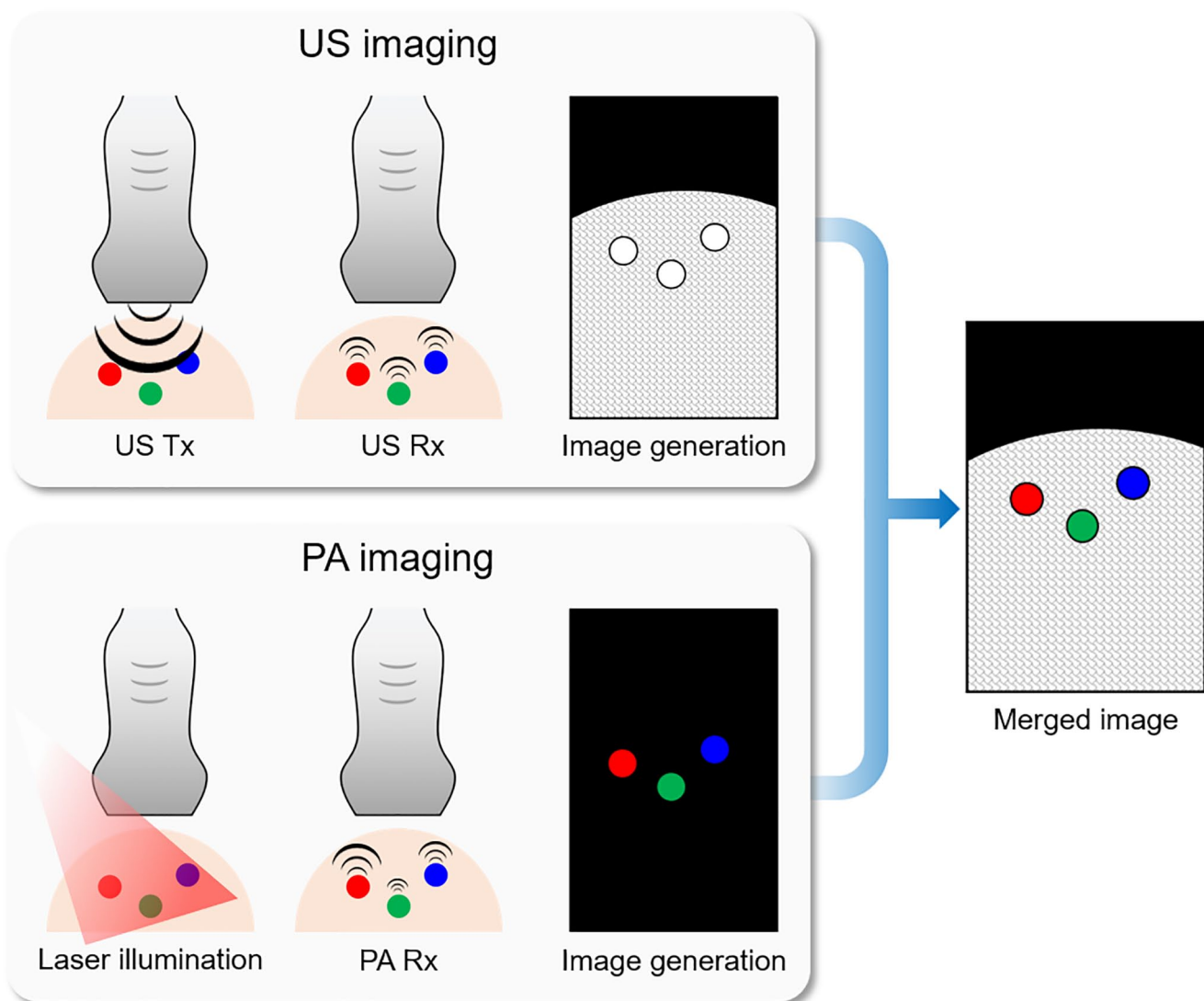
Figure 1. Schematic diagram of the signal and image generation in the US and PA imaging techniques. Conceptual results of three samples with the same morphological structure but different optical absorption properties. US: ultrasound; PA: photoacoustic; Tx: transmission; Rx: reception. (A color version of this figure is available in the online journal.)

in a single imaging platform.[9–12] The overlaid PA and US (PAUS) images can provide complementary structural and functional information about the targets (Figure 1). USI is more advantageous for visualizing morphological structures compared to PAI. However, US images suffer from low contrast owing to the speckle pattern in soft tissues. In contrast, PAI can provide strong optical contrast based on the optical absorption characteristics of the targets.[13–15] By tuning the wavelength, PAI can distinguish different samples based on their optical absorption spectra.[16–19] Due to the complementary structural and molecular functional information obtained, overlaid PAUS imaging (PAUSI) has been widely used for monitoring biological responses in various biomedical studies.[20–24]

Several commercial PAUS platforms have been used in biomedical applications. Among them, the Vintage series (Verasonics, USA) is widely utilized using the programmable platform of the system.[25,26] The programmable platforms of the Vintage series are the most advanced research

platforms that can acquire both PA and US data with flexible modifications of the operation sequence. The user can easily apply specific algorithms using a MATLAB-based software platform. However, the Vintage series is oriented to the research platform, not medical imaging applications. Therefore, clinical studies using this system might be limited without additional approval from the United States Food and Drug Administration (FDA). The VevoLAZR series (FujiFilm VisualSonics, Canada) is another commercial system for PAUSI research.[27,28] This system can provide real-time cross-sectional PAUS images with a user-friendly interface. Spectral analysis can also be performed by tuning the laser source. However, the VevoLAZR series is equipped with high-frequency (typically a center frequency of 20 MHz) US transducers because its major applications are in preclinical small animal studies. High-frequency transducers suffer from a shallow imaging depth, which is not suitable for general clinical applications. In addition, the MSOT Acuity series (iThera Medical, Germany) also have been developed
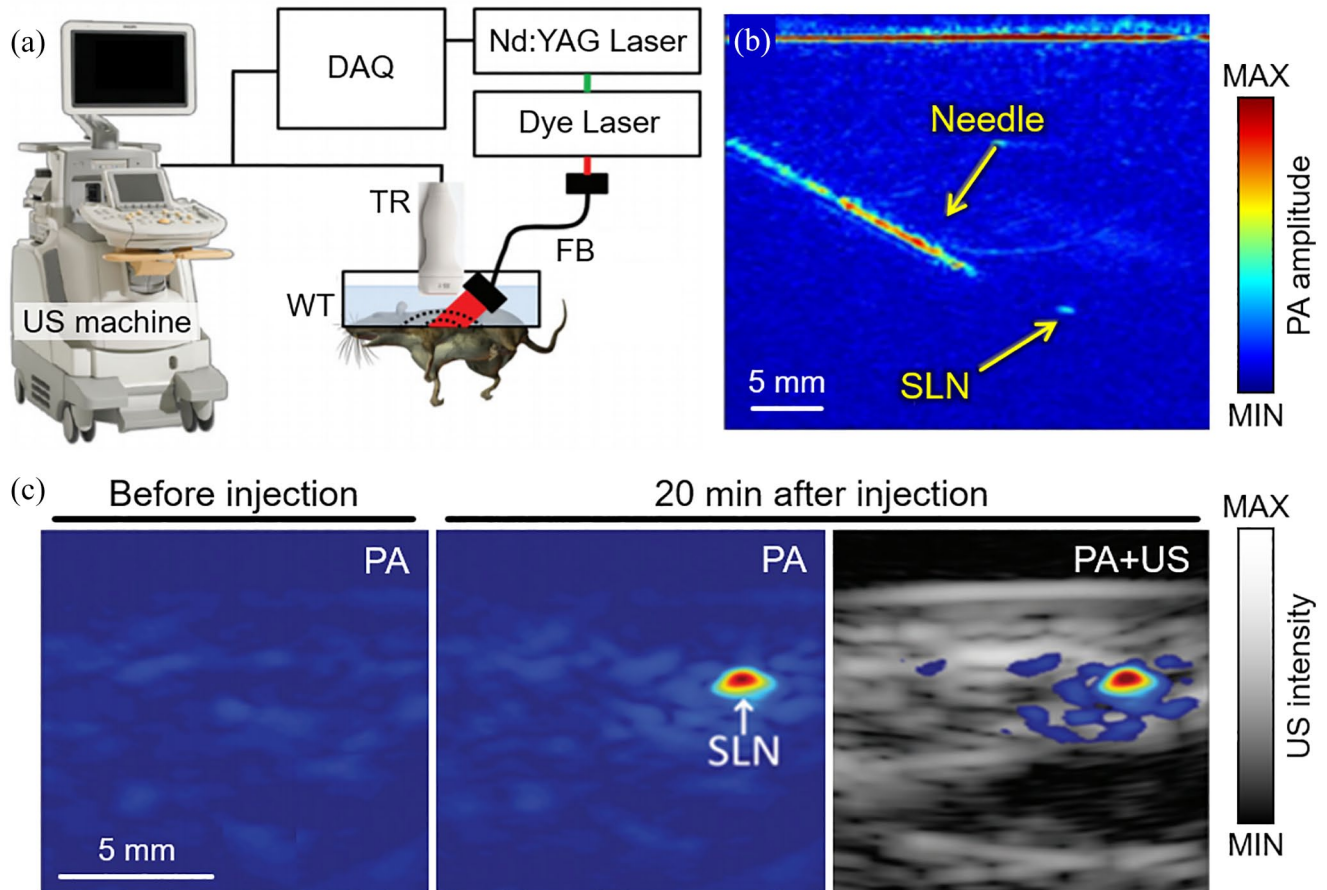
Figure 2. PA and US imaging system based on a clinical US machine. (a) Schematic diagram of the system configuration. (b) Demonstration of PA image-guided needle administration into SLN. (c) Overlaid PA and US images of SLN in a rat before and after injection of methylene blue solution. PA: photoacoustic; US: ultrasound; SLN: sentinel lymph node. The images are reproduced with permission from Kim and colleagues.[31,32] (A color version of this figure is available in the online journal.)

and applied in clinical trials using their dual-modal PAUSI capability with an arc-array transducer. This system can distinguish different chromophores by using multispectral PA responses.[29,30] However, the arc-array transducer may not be well suited for the large region due to its relatively small field of view. Moreover, the system is not suited for exploratory studies that require modification of the operation sequences in the US machine. Therefore, for the practical clinical translation of PAI, a clinical US platform with a programmable platform is required.

Here, we review our results regarding preclinical and clinical research using the PAUSI system that we implemented. The system consists of an FDA-cleared US machine and a mobile pulsed laser. The programmable platform in the US machine enables us to design operation sequences for acquiring PAUS images simultaneously. After optimizing the system, we conducted various preclinical and clinical studies. This review article focuses on the implementation, performance benchmarks, and applications of the developed PAUSI. From the results, we determined the great potential of the system for use in biomedical studies. In particular, because the system is based on clinically available machines with completely mobile structures, it has a more positive outlook in clinical applications, including cancer diagnosis, lymph node mapping, and therapy monitoring.

Photoacoustic imaging based on commercial clinical US machines

As the initial stage of the clinical PA system, we developed a PAUSI system based on a commercial clinical US machine (iU22, Phillips Healthcare, Netherlands) and then tested the feasibility of the system by applying it to the non-invasive detection of sentinel lymph node (SLN) of rats.[31,32] In the developed system, an Nd:YAG pumped dye laser beam was delivered to the imaging probe for PA wave generation (Figure 2(a)). The generated PA waves were detected using a linear-array US transducer (L8-4, Phillips Healthcare, the Netherlands). To demonstrate a clinical scenario, the needle administration of an agent into the SLN was monitored using PA and US images (Figure 2(b)). Because of the metallic substrate, the PAI clearly visualized the position of the 18-gauge needle. The SLN dyed with methylene blue was also visible in the PA images for an excitation wavelength of 650 nm and a light fluence of ~5 mJ/cm². The contrast-enhanced PA signal at the SLN was detected from PA images before and after the injection of the methylene blue solution (Figure 2(c)). The maximum detectable penetration depth was ~5.2 cm in a chicken breast tissue phantom. To test the imaging depth of the system *in vivo*, chicken breast tissue layers were stacked over the rats, and PA images were acquired

during needle insertion. The resulting images showed that the position of the needle could be successfully visualized by PAI, allowing for guidance in a minimally invasive biopsy of the SLN. However, for general clinical research, the system suffers from several limitations, such as immobile laser and unprogrammable US machine. Therefore, a clinically suitable system with a completely mobile design would be beneficial for various clinical studies.

Dual-modal PAUSI based on a programmable clinical US platform

To overcome the limitations of the previous PAUSI system, we developed a clinically applicable PAUSI system that has achieved excellent progress with real-time accessibility at high spatial and temporal resolutions.[33] The system integrated an FDA-cleared clinical US machine (EC-12R, Alpinion Medical Systems, Republic of Korea) and a portable pulsed laser (Phocus, OPOTEK, USA) (Figure 3(a)). The wavelength-tuned laser was delivered to the target sample using a fiber bundle. Then, the generated PA waves were detected using a linear-array US transducer (L3-12, Alpinion Medical Systems, Republic of Korea). By using the programmable platform in the US system, we modified the operational sequence to acquire PA and US images in real time. In brief, at every pulse illumination, the generated PA waves were detected by the US transducer and processed to reconstruct the images. To acquire US images simultaneously, conventional US imaging procedures were also conducted between the two PA image acquisition. All signal processing and image generation procedures were implemented by parallel processing algorithms using a graphics processing unit (GPU) in the US machine for real-time display. By using the fast wavelength-tuning function of the laser system, multispectral data can be acquired for spectral unmixing, which can assess functional information, including the hemoglobin oxygen saturation (sO_2) level, monitoring of agent administration, and assessment of drug delivery. Although the initially developed system showed great potential for use in clinical studies, one critical drawback diminished the clinically applicable area of the system. In the initial system, imaging parameters can only be modified after halting the image acquisition and recompiling the operational sequence.

To overcome the limitations of the initially developed system, we updated the system to enable seamless parameter modification.[34] By bypassing the parameter setting in the initialization procedure of the customized operation sequence, we developed a MATLAB-based software that can adjust all the imaging parameters in real time (Figure 3(b)). Because the software is equipped with a user-friendly graphical user interface (GUI), clinicians who are not familiar with software implementation can also use the system for their research. Representative cross-sectional PA and US images of the human thyroid region showed complementary structural and functional information. The US images clearly visualized the morphology of the thyroid and the surrounding tissues (gray-scaled image in Figure 3(b)), while the PA images (pseudo-colored image in Figure 3(b)) delineated the blood vessels based on the optical absorption characteristics.

In addition to the parameter modification platform, we updated the imaging probe for more efficient light delivery. The optical fluence in biological tissue was evaluated using Monte Carlo simulations of photon diffusion. Based on the simulation results, we concluded that the distance between the laser beam and the imaging plane at the surface of the imaging sample (Δd) determines the light delivery efficiency rather than the incident angle of the laser. Therefore, we updated the adapter for the imaging probe to minimize the Δd (Figure 3(c)). Compared to the initial design ($\Delta d = 10$ mm), the updated design was equipped with a standoff to make Δd sufficiently small. More recently, we finalized the probe design to be more suitable for handheld operations in clinical settings.[35]

While the developed system visualizes cross-sectional images, the landscape images would provide intuitive information, such as the blood vessel network. A typical method for acquiring transversal images is the maximum amplitude projection (MAP) of signals along the depth direction. For MAP, volumetric data with elevational scanning of the linear-array transducer should be acquired. In response, we developed a handheld scanner that operates with a scanning range of 38.4 mm (Figure 3(d)).[36] The Scotch yoke mechanism, which converts rotation into a linear reciprocating motion, was implemented. The developed scanner was available for handheld operation in a compact size ($100 \times 80 \times 100$ mm³) and weight (950 g). The distance between the laser beam and the imaging plane was minimized by adding a standoff filled with water. During the scans, the PA and US data were stored in the flash memory of the US machine and then transferred to the data processing unit to generate volumetric images. In particular, because the entire handheld scanner can be positioned in any direction without spilling the water, it can be used to acquire volumetric images from various parts of the human body, such as the neck, wrist, and thighs (Figure 3(e)), which are otherwise difficult to image using previously developed imaging systems.

Preclinical applications of the PAUSI system

To evaluate the capability of the system for biomedical research, we explored preclinical small animal studies using the developed PAUSI system. In particular, we verified the deep-tissue imaging ability of PAI with exogenous contrast agents that absorb light in the NIR (NIR-II) window. The NIR-II light has advantages for deep-tissue imaging: less light scattering and relatively low light absorption. Therefore, the NIR-II light can be delivered to a deeper position in biological tissue than light of shorter wavelengths. Although the improved penetration depth is beneficial, the absence of an appropriate agent material for absorbing light in the NIR-II window had previously been considered an obstacle for further studies. In our previous studies, we presented *in vivo* imaging results using nanoparticles that absorb the NIR-II light. As a first study, we synthesized Bi_2Se_3 nanoplates that exhibited relatively strong PA signals at 1064 nm.[14] The deep-tissue imaging capability was evaluated by acquiring PA signals of Bi_2Se_3 containing a silicone tube buried under stacks of chicken breast tissue (Figure 4(a)). The *in vitro* study showed
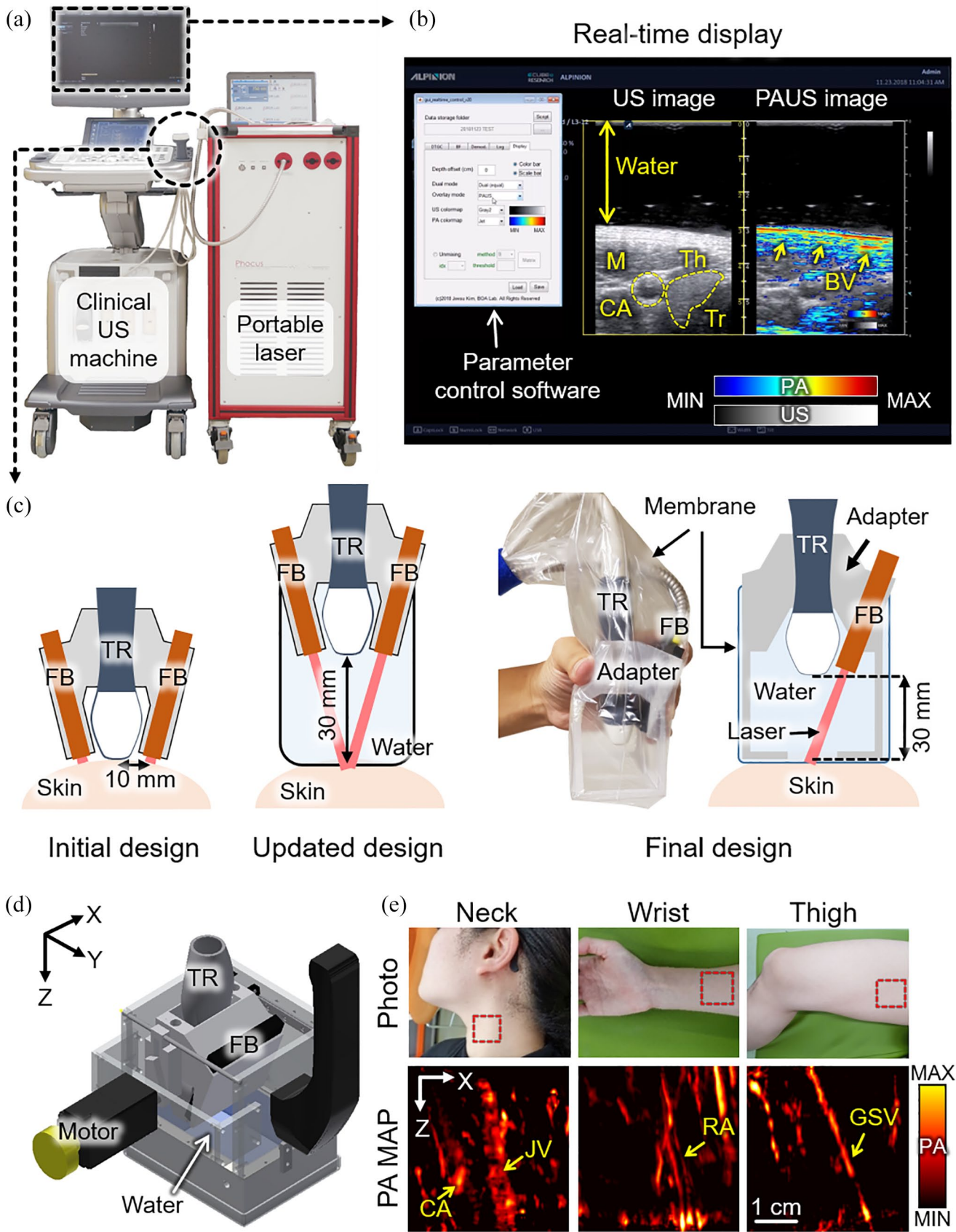
Figure 3. Clinically available PA and US imaging system based on a programmable clinical US machine. (a) Photograph of the system. (b) Real-time display of PA and US images of the human thyroid region *in vivo*. Inset image shows the real-time parameter control software developed using MATLAB-based software. (c) Schematic illustration of the development of the imaging probe. (d) Schematic illustration of the handheld scanner used to acquire volumetric data. (e) Representative results of volumetric PA images from various parts of the human body. PA: photoacoustic; US: ultrasound; M: muscle; Th: thyroid; CA: carotid artery; JV: jugular vein; RA: radial artery; GSV: great saphenous; Tr: trachea; BV: blood vessel; FB: fiber bundle; TR: transducer; MAP: maximum amplitude projection. The images are reproduced with permission from Kim and colleagues.[33–36] (A color version of this figure is available in the online journal.)
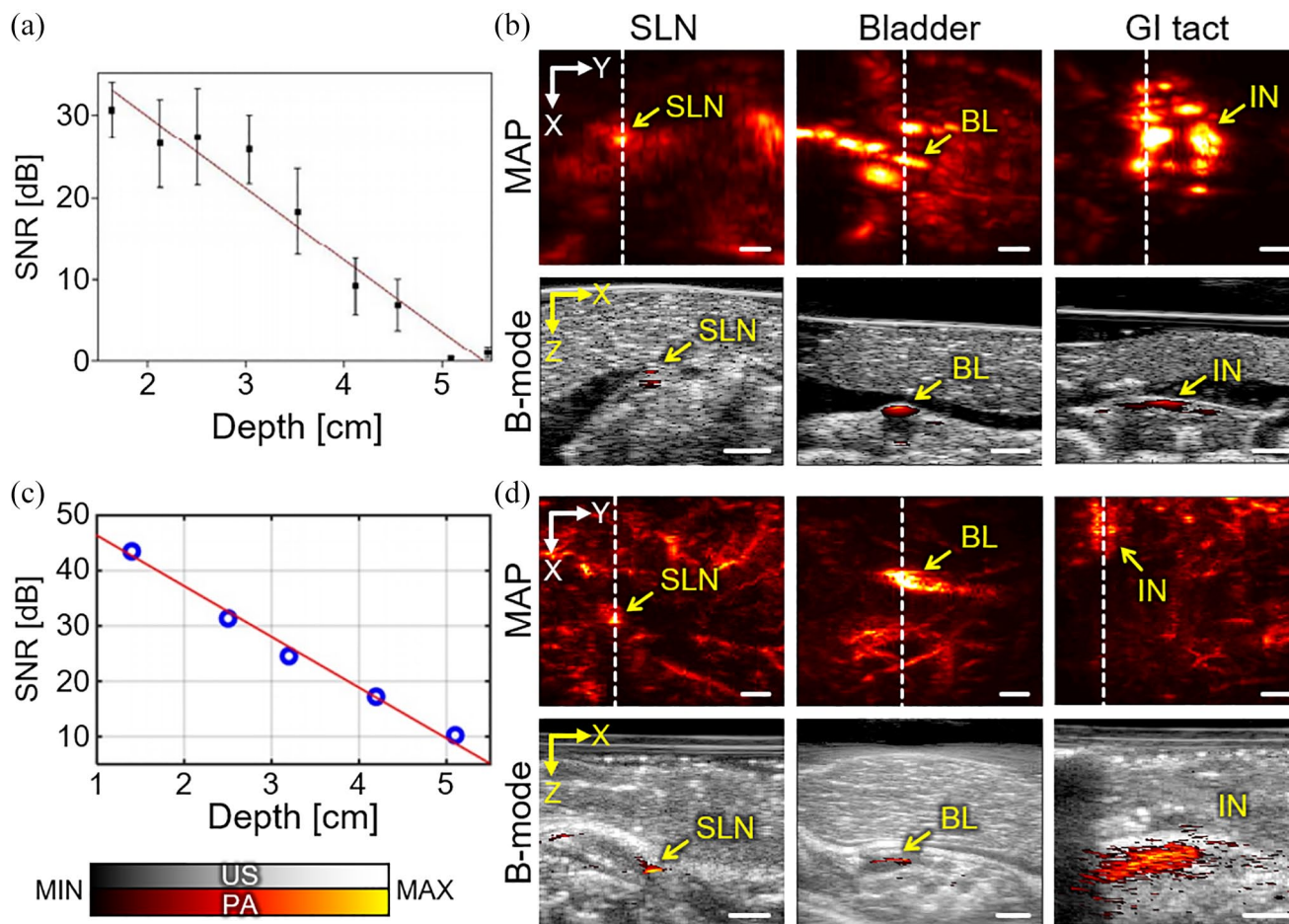
Figure 4. Preclinical deep-tissue imaging with the developed PA and US imaging system. (a) *In vitro* evaluation of imaging depth with PA signals from Bi_2Se_3 samples buried in chicken tissue layers. (b) Contrast-enhanced PA MAP and cross-sectional B-mode images of mice *in vivo*. Images were taken after injection of Bi_2Se_3 nanoplates. (c) PA signal detection from NiPNP samples in chicken tissue layers. (d) PA images of rats *in vivo*, after injection of NiPNP solutions. PA: photoacoustic; US: ultrasound; NiPNP: nickel dithiolene-based polymeric nanoparticle; SNR: signal-to-noise ratio; SLN: sentinel lymph node; BL: bladder; IN: intestine; GI: gastrointestinal; MAP: maximum amplitude projection. The images are reproduced with permission from Park and colleagues.[14,37] (A color version of this figure is available in the online journal.)

an imaging depth of up to 5.3 cm can be acquired with a concentration of 15.26 mg/mL. In addition, we assessed the *in vivo* imaging ability of the contrast-enhanced sentinel lymph node (SLN), bladder, and gastrointestinal (GI) tract in mice (Figure 4(b)). The images were acquired before and after the injection of Bi_2Se_3 solutions through transurethral and oral injections for bladder and GI tract imaging, respectively. To validate the deep-tissue imaging capability, we stacked layers of chicken breast tissue on top of the mice. An imaging depth of ~1.2 cm with sufficient PA contrast was achieved for both *in vivo* experiments. We conducted a similar study with another contrast agent, nickel dithiolene-based polymeric nanoparticles (NiPNP), which also absorbs light in the NIR-II window (1000–1350 nm).[37] Compared with previous Bi_2Se_3 nanoplates, NiPNP has an absorption peak at 1064 nm, which is highly favorable for PAI. Similar to the previous experiments, the NiPNP-containing tube showed a maximum measurable depth of ~5.1 cm under the chicken tissue layers (Figure 4(c)). The *in vivo* experiments also verified the deep-tissue imaging capability of the SLN, GI tract, and bladder of rats, with an imaging depth of ~1.5 cm (Figure 4(d)). The results show that our developed PAUSI system is

capable of deep-tissue imaging and is a promising tool for *in vivo* preclinical PAUSI studies.

Clinical applications of the PAUSI system

The developed PAUSI system has also been used in clinical studies, especially for detecting cancers using intrinsic chromophores, such as melanin, oxy-hemoglobin, and deoxy-hemoglobin. Based on the strong melanin contrast, PAI can efficiently visualize the boundary of melanoma, which is one of the most common skin cancers. To test the feasibility of the system for visualizing the melanoma region, we acquired *ex vivo* images of the extracted tissues from melanoma patients[38] (Figure 5(a)). The results successfully delineated PA signals from melanoma and marker pen using multiple wavelengths. Although *ex vivo* imaging showed promising results, *in vivo* imaging and depth assessment are necessary for clinical use. Therefore, we developed a handheld 3D imaging probe for the *in vivo* imaging of melanoma.[36] The developed probe can generate volumetric images using the Scotch yoke mechanism. Using
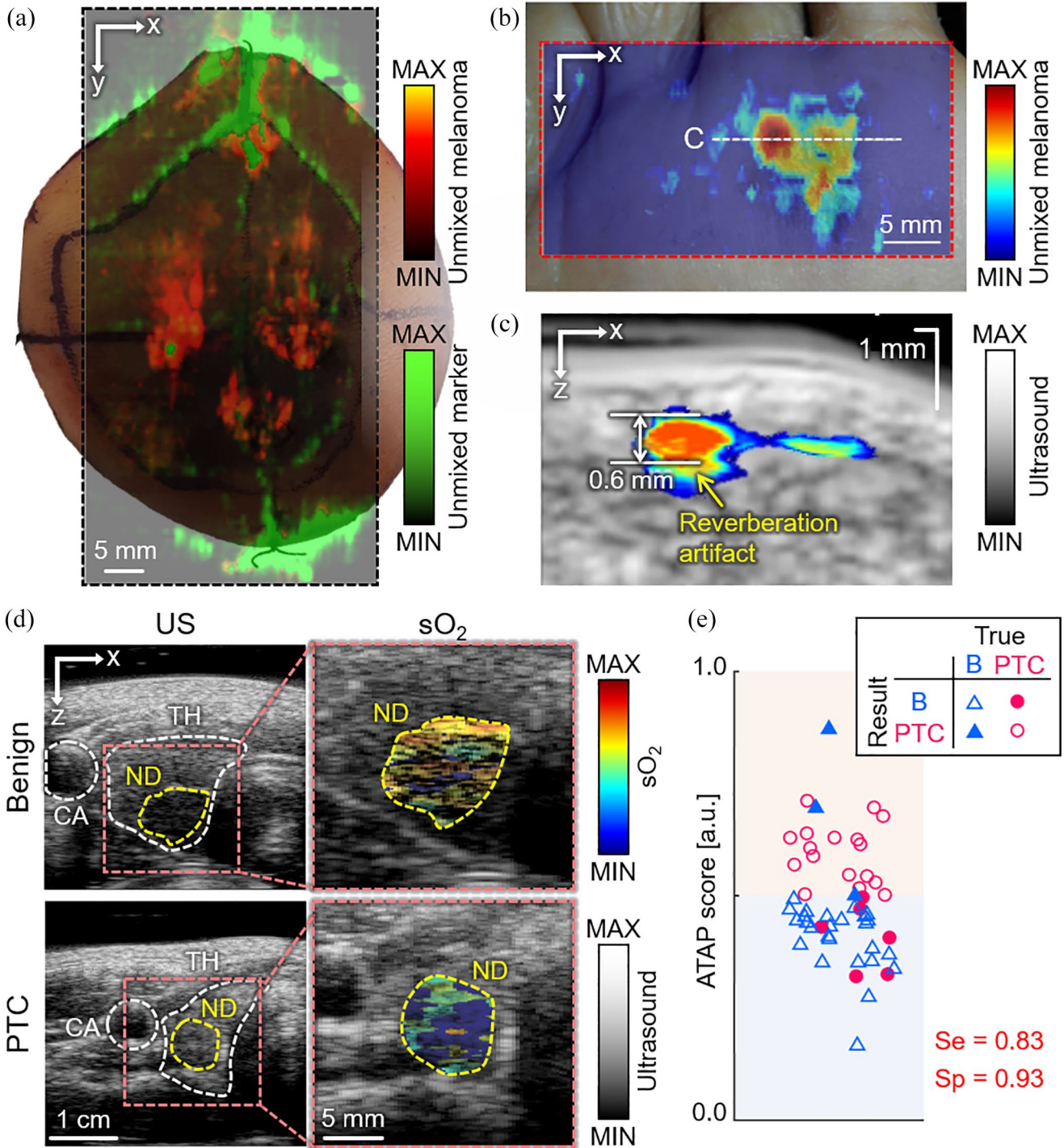
Figure 5. Multispectral PA imaging results of cancer region *in vivo*. (a) Multispectral PA images delineating melanoma and marker pen in excised human tissue. (b) Maximum amplitude projection of melanoma signal from the spectral unmixing of the multispectral PA responses *in vivo*. (c) Cross-sectional PA and US image of the position of white dashed line in (b). (d) sO$_2$ distribution in thyroid nodules from the representative benign and PTC patients. (e) Classification result of thyroid nodules using a novel ATAP scoring method. Red and blue area denote decision results as PTC and benign, respectively. PA: photoacoustic; US: ultrasound; PTC: papillary thyroid cancer; B: benign; sO$_2$: hemoglobin oxygen saturation; CA: carotid artery; TH: thyroid; ND: nodule; ATAP: the American Thyroid Association and the photoacoustic probability of PTC; Se: sensitivity; Sp: specificity. The images are reproduced with permission from Kim and colleagues.[35,38,39] (A color version of this figure is available in the online journal.)

the 3D imaging probe, we acquired *in vivo* PAUS images of melanoma in patients and then assessed the melanoma components using spectral unmixing of the multispectral PA signals[39] (Figure 5(b)). From the cross-sectional images (Figure 5(c)), we could measure the depth of the lesion, which matched well with the histological results. Because it is critical to know the exact boundary of melanoma under the skin surface for efficient surgical operation, the PAUSI system would serve an important role in determining the boundary and deciding on the excision region of melanoma

Table 1. Summary of preclinical and clinical studies using PAUSI system based on clinical US machines.

Application	US system (manufacturer)	Imaging probe (bandwidth)	Scanner	Imaging target	Ref.
Preclinical	iU22 (Philips Healthcare)	Linear array (4–8 MHz)	NA	MB delivered SLN in rats	Kim et al.[31]
	iU22 (Philips Healthcare)	Phased array (1–5 MHz) Linear array (4–8, 7–15 MHz)	Motorized scanner	MB delivered SLN in rats	Erpelding et al.[32]
	EC12R (Alpinion Medical Systems)	Linear array (3–12 MHz)	Motorized scanner	Bi₂Se₃ delivered bladders, GI tracts, and SLN in mice	Park et al.[14]
	EC12R (Alpinion Medical Systems)	Linear array (3–12 MHz)	Motorized scanner	NiPNP delivered bladders, GI tracts, and SLN in rats	Park et al.[37]
	EC12R, VIFU2000 (Alpinion Medical Systems)	Linear array (8–17 MHz)	NA	Xenografted melanoma tissues in mice	Kim et al.[40]
	EC12R (Alpinion Medical Systems)	Linear array (3–12 MHz)	NA	Livers in rats	Choi et al.[41]
Clinical	EC12R (Alpinion Medical Systems)	Linear array (3–12 MHz)	NA	Thyroid nodules in human	Kim et al.[35]
	EC12R (Alpinion Medical Systems)	Linear array (3–12 MHz)	Motorized scanner	Excised melanoma tissues from human	Kim et al.[38]
	EC12R (Alpinion Medical Systems)	Linear array (3–12 MHz)	Motorized handheld scanner	Melanoma tissues in human	Park et al.[39]
	EC12R (Alpinion Medical Systems)	Linear array (3–12 MHz)	Motorized scanner	Peripheral vasculature in human feet	–

PAUSI: photoacoustic and ultrasound imaging; US: ultrasound; NA: not applicable; MB: methylene blue; NiPNP: nickel dithiolene-based polymeric nanoparticle; SLN: sentinel lymph node; GI: gastrointestinal.

in vivo. In addition to melanoma, we also applied the PAUSI system to triage thyroid nodules by multiparametric analysis of multispectral PA responses *in vivo*.[35] Multispectral PA and US images were acquired from the recruited patients who had papillary thyroid cancer (PTC) or benign nodules at excitation wavelengths of 700, 756, 796, 866, and 900 nm. From the multispectral PA response, the sO_2 levels in the thyroid nodules were visualized (Figure 5(d)). The results show that benign patients tend to have higher sO_2 values, while PTC patients have lower sO_2 values. For the multiparametric analysis, we quantified three parameters: average sO_2 value, skew angle in sO_2 distribution, and PA spectral gradient. As a result, we calculated the probability of PTC based on the parameters and then proposed a novel scoring method by combining it with the American Thyroid Association guideline score, which is a typical method of triaging nodules based on US images. The proposed ATAP (P for PA) score could classify benign and PTC nodules with a sensitivity of 83% and a specificity of 93%. The results reported the first statistical assessment based on the multiparametric analysis of multispectral PA signals from thyroid cancer patients, showing the great potential of our method, which can be used as a complementary tool for triaging thyroid nodules in clinical settings.

Conclusions

In this article, we review preclinical and clinical studies using our PAUSI system. The system is based on an FDA-cleared general-purpose US machine and a portable laser, which can be readily adapted to various clinical scenarios. The programmable architecture of the US machine enables users to design and optimize PAUS scans for specific purposes. Various functions have been implemented, including conventional US B-mode, PA B-mode, functional PA imaging (e.g. sO_2 mapping), and motorized volume scanning for various applications including image-guided biopsy, SLN detection, GI tract, and diagnostic imaging of human melanoma and thyroid nodules. These studies have successfully demonstrated the capability of the developed PAUSI system for providing complementary PA contrast on top of US images, thereby providing clinically relevant biological information in a radiation-free, non-invasive, and real-time manner. One limitation of our previous clinical studies that has to be addressed is the lack of diversity in skin color. All the subjects we recruited were Asian, especially Korean. The skin color may affect the quality of the resulting images because the darker skin absorbs more laser power and reduces optical fluence compared to the brighter skin. Therefore, one of our future studies would be the assessment of PA signal quality according to skin colors.

Several studies using the PAUSI system are in progress and raise the possibility of extending its clinical applications. The feasibility of 3D multistructural imaging of human feet has been demonstrated using co-registered PA and US images. Various structural information (i.e. skin, bone, and vessel) was visualized from US volumes and combined with high-resolution vasculature and sO_2 maps from PA volumes. We also demonstrated the potential of the system for real-time PA thermometry during high-intensity focused ultrasound (HIFU) treatment.[40] The PA amplitude was proportional to the temperature measured by a thermocouple in both phantoms and *in vivo* tumor-bearing mice. Using a lipid-sensitive continuous-wave laser instead of a photoacoustic pulsed laser, non-invasive photothermal strain imaging of fatty liver was successfully performed through *in vivo* and *ex vivo* studies on rats.[41] Table 1 summarizes the studies based on the applications of our PAUSI system to date.

In current medical practice, sonography is widely and routinely used for diagnosis and therapeutic procedures because of its real-time imaging capability, portability, safety, non-invasiveness, and so on. As summarized in this review,

the PAUSI system can be used as a conventional ultrasound scanner and complement its lack of molecular functional information. Therefore, we believe that this system can be used to provide new clinical information in diagnostic and therapeutic applications in the near future.

From the previous clinical studies, we realized that the key issue for the successful clinical translation of the system is user-friendly operation, such that clinicians or radiologists can use the system by themselves. From the user's point of view, there are several requirements that the current PAUSI system should address including (1) real-time quantification of the multispectral PA responses, (2) enhanced US B-mode image quality, (3) compact, or embedded laser for better mobility, and (4) miniaturized imaging probe. By solving these issues, the system can be acceptable to be used in the clinical world.

AUTHORS' CONTRIBUTIONS

All authors participated in the critical reading and writing of the manuscript; JK and CK conceived and supervised the project and wrote the manuscript. E-YP, HL, and SH prepared, reviewed, and analyzed previously reported articles, prepared figures, and wrote the manuscript. *These authors contributed equally to this work.

DECLARATION OF CONFLICTING INTERESTS

The author(s) declared the following potential conflicts of interest with respect to the research, authorship, and/or publication of this article: Chulhong Kim has financial interests in OPTICHO, which, however, did not support this work.

ORCID ID

Chulhong Kim [iD] https://orcid.org/0000-0001-7249-1257

REFERENCES

1. Kagadis GC, Loudos G, Katsanos K, Langer SG, Nikiforidis G. In vivo small animal imaging: current status and future prospects. *Med Phys* 2010;**37**:6421–42
2. Kim C, Favazza C, Wang LV. In vivo photoacoustic tomography of chemicals: high-resolution functional and molecular optical imaging at new depths. *Chem Rev* 2010;**110**:2756–82
3. Bell AG. The photophone. *Science* 1880;**1**:130–4
4. Steinberg I, Kim J, Schneider MK, Hyun D, Zlitni A, Hopper SM, Klap T, Sonn GA, Dahl JJ, Kim C. Superiorized photo-acoustic Non-NEgative reconstruction (SPANNER) for clinical photoacoustic imaging. *IEEE Trans Med Imaging* 2021;**40**:1888–97
5. Cho S, Jeon S, Choi W, Managuli R, Kim C. Nonlinear pth root spectral magnitude scaling beamforming for clinical photoacoustic and ultrasound imaging. *Opt Lett* 2020;**45**:4575–8
6. Jeon S, Choi W, Park B, Kim C. A deep learning based model that reduces speed of sound aberrations for improved in vivo photoacoustic imaging. *IEEE Trans Image Process* 2021;**30**:8773–84
7. Jeon S, Park E-Y, Choi W, Managuli R, Jong Lee K, Kim C. Real-time delay-multiply-and-sum beamforming with coherence factor for in vivo clinical photoacoustic imaging of humans. *Photoacoustics* 2019;**15**:100136
8. Choi W, Oh D, Kim C. Practical photoacoustic tomography: realistic limitations and technical solutions. *J Appl Phys* 2020;**127**:230903
9. Steinberg I, Huland DM, Vermesh O, Frostig HE, Tummers WS, Gambhir SS. Photoacoustic clinical imaging. *Photoacoustics* 2019;**14**:77–98
10. Choi W, Park E-Y, Jeon S, Kim C. Clinical photoacoustic imaging platforms. *Biomed Eng Lett* 2018;**8**:139–55
11. Park J, Park B, Kim T, Jung S, Choi W, Ahn J, Yoon D, Kim J, Jeon S, Lee D. Quadruple ultrasound, photoacoustic, optical coherence, and fluorescence fusion imaging with a transparent ultrasound transducer. *Proc Natl Acad Sci USA* 2021;**118**:e1920879118
12. Park B, Han M, Park J, Kim T, Ryu H, Seo Y, Kim WJ, Kim HH, Kim C. A photoacoustic finder fully integrated with a solid-state dye laser and transparent ultrasound transducer. *Photoacoustics* 2021;**23**:100290
13. Park E-Y, Park S, Lee H, Kang M, Kim C, Kim J. Simultaneous dual-modal multispectral photoacoustic and ultrasound macroscopy for three-dimensional whole-body imaging of small animals. *Photonics* 2021;**8**:13
14. Park S, Park G, Kim J, Choi W, Jeong U, Kim C. Bi2Se3 nanoplates for contrast-enhanced photoacoustic imaging at 1064 nm. *Nanoscale* 2018;**10**:20548–58
15. Zhang Y, Jeon M, Rich LJ, Hong H, Geng J, Zhang Y, Shi S, Barnhart TE, Alexandridis P, Huizinga JD. Non-invasive multimodal functional imaging of the intestine with frozen micellar naphthalocyanines. *Nat Nanotechnol* 2014;**9**:631–8
16. Lee C, Kim J, Zhang Y, Jeon M, Liu C, Song L, Lovell JF, Kim C. Dual-color photoacoustic lymph node imaging using nanoformulated naphthalocyanines. *Biomaterials* 2015;**73**:142–8
17. Taruttis A, Ntziachristos V. Advances in real-time multispectral optoacoustic imaging and its applications. *Nat Photon* 2015;**9**:219–27
18. Lee C, Jeon M, Jeon MY, Kim J, Kim C. In vitro photoacoustic measurement of hemoglobin oxygen saturation using a single pulsed broadband supercontinuum laser source. *Appl Opt* 2014;**53**:3884–9
19. Baik JW, Kim H, Son M, Choi J, Kim KG, Baek JH, Park YH, An J, Choi HY, Ryu SY. Intraoperative label-free photoacoustic histopathology of clinical specimens. *Laser Photon Rev* 2021;**15**:2100124
20. Kim J, Lee D, Jung U, Kim C. Photoacoustic imaging platforms for multimodal imaging. *Ultrasonography* 2015;**34**:88–97
21. Ahn J, Kim JY, Choi W, Kim C. High-resolution functional photoacoustic monitoring of vascular dynamics in human fingers. *Photoacoustics* 2021;**23**:100282
22. Baik JW, Kim JY, Cho S, Choi S, Kim J, Kim C. Super wide-field photoacoustic microscopy of animals and humans in vivo. *IEEE Trans Med Imag* 2019;**39**:975–84
23. Jeon S, Kim J, Lee D, Baik JW, Kim C. Review on practical photoacoustic microscopy. *Photoacoustics* 2019;**15**:100141
24. Kim J, Kim JY, Jeon S, Baik JW, Cho SH, Kim C. Super-resolution localization photoacoustic microscopy using intrinsic red blood cells as contrast absorbers. *Light Sci Appl* 2019;**8**:103–11
25. Yuan J, Xu G, Yu Y, Zhou Y, Carson PL, Wang X, Liu X. Real-time photoacoustic and ultrasound dual-modality imaging system facilitated with graphics processing unit and code parallel optimization. *J Biomed Opt* 2013;**18**:86001
26. Kothapalli S-R, Sonn GA, Choe JW, Nikoozadeh A, Bhuyan A, Park KK, Cristman P, Fan R, Moini A, Lee BC, Wu J, Carver TE, Trivedi D, Shiiba L, Steinberg I, Huland DM, Rasmussen MF, Liao JC, Brooks JD, Khuri-Yakub PT, Gambhir SS. Simultaneous transrectal ultrasound and photoacoustic human prostate imaging. *Sci Transl Med* 2019;**11**:1–12
27. Needles A, Heinmiller A, Sun J, Theodoropoulos C, Bates D, Hirson D, Yin M, Foster F. Development and initial application of a fully integrated photoacoustic micro-ultrasound system. *IEEE Trans Ultrason Ferroelectr Freq Control* 2013;**60**:888–97

28. Zafar H, Breathnach A, Subhash HM, Leahy M. Linear-array-based photoacoustic imaging of human microcirculation with a range of high frequency transducer probes. *J Biomed Opt* 2015;**20**:051021

29. Levi J, Sathirachinda A, Gambhir SS. A high-affinity, high-stability photoacoustic agent for imaging gastrin-releasing peptide receptor in prostate cancer. *Clin Cancer Res* 2014;**20**:3721–9

30. Becker A, Masthoff M, Claussen J, Ford SJ, Roll W, Burg M, Barth PJ, Heindel W, Schafers M, Eisenblatter M, Wildgruber M. Multispectral optoacoustic tomography of the human breast: characterisation of healthy tissue and malignant lesions using a hybrid ultrasound-optoacoustic approach. *Eur Radiol* 2018;**28**:602–9

31. Kim C, Erpelding TN, Jankovic L, Pashley MD, Wang LV. Deeply penetrating in vivo photoacoustic imaging using a clinical ultrasound array system. *Biomed Opt Exp* 2010;**1**:278–84

32. Erpelding TN, Kim C, Pramanik M, Jankovic L, Maslov K, Guo Z, Margenthaler JA, Pashley MD, Wang LV. Sentinel lymph nodes in the rat: noninvasive photoacoustic and US Imaging with a Clinical US System 1. *Radiology* 2010;**256**:102–10

33. Kim J, Park S, Jung Y, Chang S, Park J, Zhang Y, Lovell JF, Kim C. Programmable real-time clinical photoacoustic and ultrasound imaging system. *Sci Rep* 2016;**6**:35137

34. Kim J, Park E-Y, Park B, Choi W, Lee KJ, Kim C. Towards clinical photoacoustic and ultrasound imaging: probe improvement and real-time graphical user interface. *Exp Biol Med* 2020;**245**:321–9

35. Kim J, Park B, Ha J, Steinberg I, Hooper SM, Jeong C, Park E-Y, Choi W, Liang T, Bae J-S. Multiparametric photoacoustic analysis of human thyroid cancers in vivo. *Cancer Res* 2021;**81**:4849–60

36. Lee C, Choi W, Kim J, Kim C. Three-dimensional clinical handheld photoacoustic/ultrasound scanner. *Photoacoustics* 2020;**18**:100173

37. Park B, Lee KM, Park S, Yun M, Choi H-J, Kim J, Lee C, Kim H, Kim C. Deep tissue photoacoustic imaging of nickel (II) dithiolene-containing polymeric nanoparticles in the second near-infrared window. *Theranostics* 2020;**10**:2509–21

38. Kim J, Kim YH, Park B, Seo HM, Bang CH, Park GS, Park YM, Rhie JW, Lee JH, Kim C. Multispectral ex vivo photoacoustic imaging of cutaneous melanoma for better selection of the excision margin. *Br J Dermatol* 2018;**179**:780–2

39. Park B, Bang CH, Lee C, Han JH, Choi W, Kim J, Park GS, Rhie JW, Lee JH, Kim C. 3D wide-field multispectral photoacoustic imaging of human melanomas in vivo: a pilot study. *Journal of the European Academy of Dermatology and Venereology* 2020;**35**:669–76

40. Kim J, Choi W, Park E-Y, Kang Y, Lee KJ, Kim HH, Kim WJ, Kim C. Real-time photoacoustic thermometry combined with clinical ultrasound imaging and high intensity focused ultrasound. *IEEE Trans Biomed Eng* 2019;**66**:3330–8

41. Choi C, Choi W, Kim J, Kim C. Non-invasive photothermal strain imaging of non-alcoholic fatty liver disease in live animals. *IEEE Trans Med Imaging* 2021;**40**:2487–95